AAS 16-483

POTENTIAL EFFECTS OF A REALISTIC SOLAR SAIL AND COMPARISON TO AN IDEAL SAIL

Jules Simo* **and Colin R. McInnes†**

Solar sail technology offers new capabilities for space missions due to the opportunities for non-Keplerian orbits. In this paper, novel families of highly non-Keplerian orbits for spacecraft utilising solar sail at linear order are investigated in the Earth-Moon circular restricted three-body problem. Firstly, it is assumed implicitly that the solar sail is a perfect reflector. Based upon the first-order approximation, an analytical formulation of the periodic orbits at linear order is presented. The approximate analytical solutions offer useful insights into the nature of the motion in the vicinity of the libration points, and are used to give periodic solutions numerically in the full nonlinear system. These orbits were accomplished by using an optimal choice of the sail pitch angle, which maximize the out-of-plane distance. Thereafter, the resulting effects of the non-ideal flat sail model have been computed and compared with an ideal solar sail. A square sail configuration, which is likely to be chosen for various near-term sail missions is used to illustrate the concept. The main effect of the non-perfect sail is to reduce the out-of-plane displacement distance which may be achieved for a given characteristic acceleration. It is also observed that there is a significant deviation in force magnitude between the realistic solar sail and the ideal solar sail model.

INTRODUCTION

Now more than a speculative technology, solar sailing offers new capabilities for the design of space missions. This new concept promises to be useful in overcoming the challenges of transportation throughout the solar system. By exploiting the momentum transported by solar photons, solar sails can perform new high-energy mission concepts, which are essentially impossible for conventional propulsion, without the need for reaction mass. A practical concern for other forms of low-thrust propulsion is the limited mission duration, which is fixed by the propellant mass fraction of the spacecraft.[1,2,3,4,5,6,7,8,9,10,11,12,13,14] For these reasons, solar sails with a large propellantless ΔV capability can provide a wide range of opportunities for innovative low-cost missions.

A solar sailing mission architecture with a solar sail loading (mass per unit area) of only $1.5\ gm^{-2}$ would enable solar physics missions that could levitate above the solar poles, providing continuous observations or hovering at any particular location in the solar system. Such a solar sail could also displace circular heliocentric orbits high above the ecliptic plane, where the orbit period is chosen to be synchronous with the Earth or some other solar system body. Solar radiation pressure also impacts the location of the libration points. Consequently, the libration points of the Earth-Sun system can be artificially displaced using a modest solar sail. A case study example is the location

*Lecturer & Course Leader for MEng/BEng (Hons) Aerospace Engineering, School of Engineering, University of Central Lancashire, Preston, PR1 2HE, United Kingdom. Email: jsimo@uclan.ac.uk.

†James Watt Chair, Professor of Engineering Science, School of Engineering, University of Glasgow, Glasgow, G12 8QQ, United Kingdom. Email: colin.mcinnes@glasgow.ac.uk.

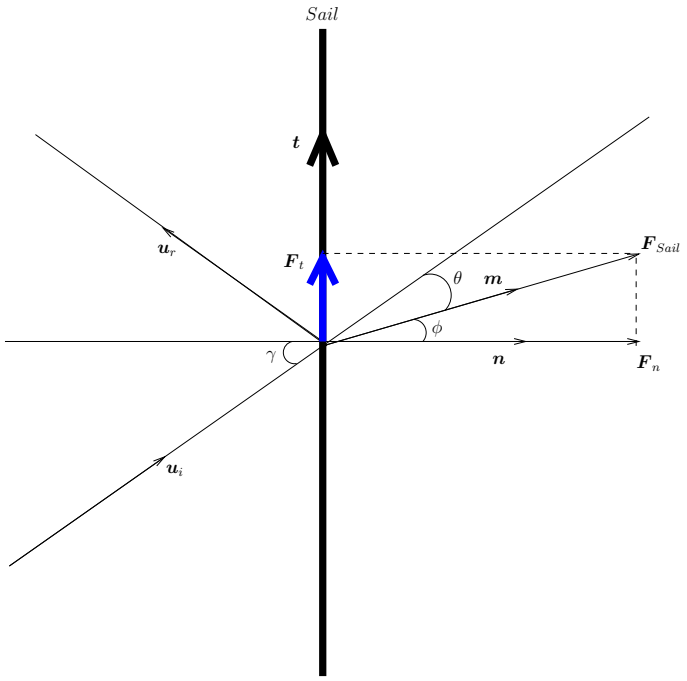

Figure 1. Representative forces on a non-perfectly reflecting solar sail.

of the L_1 point, that can be displaced closer to the Sun or even above the plane of the Earth's orbit. The proposed new sunward equilibrium location formed the basis for the NASA/NOAA Geostorm mission concept.

In this work, novel families of highly non-Keplerian orbits (NKO) for spacecraft utilising solar sail at linear order are investigated in the Earth-Moon circular restricted three-body problem (CRTBP).[1,15,16,17,18,2,3,4,19,20] Throughout this paper, the sail optical parameters for a 100×100 m square solar sail will be used to compare the optical solar sail model (realistic solar sail model) to an ideal solar sail. A particular use of such orbits includes continuous communications between the equatorial regions of the Earth and the lunar poles to support future robotic and human exploration.[21,22,23,24]

FORCE ON A NON-PERFECTLY REFLECTING SOLAR SAIL

The assumption of an ideal flat solar sail can render the model inaccurate, since for a realistic solar sail the effects of an imperfect reflector can be considered in the model. A significant feature for the non-perfect flat solar sail is that the so-called cone angle reaches a maximum, limiting the operational range of the solar sail, whereas for the ideal sail the thrust vector is always oriented normal to the sail surface and can in principle be operated up to a 90° Sun angle. In a prior study, it was assumed implicitly that the solar sail is a perfect reflector. Thus, by adding the force due to the incident and reflected photons, the resulting force exerted on the solar sail is directed normal to the sail surface. This is in contrast to the non-ideal flat sail model, where one component of the force is along the sail surface, and so the combined force is no longer normal to the sail surface. As can be seen in Figure 1, the force exerted on the solar sail has a normal component F_n and a transversal component F_t.

The force due to absorption is denoted by $\boldsymbol{F}_a$ and the force $\boldsymbol{F}_e$ from re-radiated photons as would be computed from thermodynamics will be defined by a vector $\boldsymbol{n}$ normal to the sail surface.

By making use of the reflectance, absorption and emissitivity of the sail film, the total force acting on the solar sail due to the solar radiation pressure is given by

$$\boldsymbol{F}_{Sail} = \boldsymbol{F}_r + \boldsymbol{F}_a + \boldsymbol{F}_e, \tag{1}$$

where the force due to reflection $\boldsymbol{F}_r$ is the sum of a fraction s due to specular reflection acting along the normal and the transverse directions and a fraction $B_f(1-s)$ due to diffuse reflection acting along the normal direction. It should be noted that B_f is the non-Lambertian coefficient of the front surface of the sail and s a fraction of specularly reflected photons.

The total force will depend upon the optical characteristics of the sail film, which can be parameterised by the reflection coefficient $\tilde{\rho}$, the absorption coefficient a and the transmission coefficient τ such that

$$\tilde{\rho} + a + \tau = 1. \tag{2}$$

Since the transmission coefficient $\tau = 0$ on the reflecting side of the sail, the absorption coefficient is given by

$$a = 1 - \tilde{\rho}. \tag{3}$$

The direction of incidence of photons will be defined by a unit vector $\boldsymbol{u}_i$ and the direction of specularly reflected photons by a unit vector $\boldsymbol{u}_r$.

The total force exerted on the solar sail is obtained after decomposing the forces involved into their normal and transverse components as

$$\begin{aligned} \boldsymbol{F}_n &= PA\Big[(1+\tilde{\rho}s)\cos^2(\gamma) + B_f(1-s)\tilde{\rho}\cos(\gamma) \\ &\quad +(1-\tilde{\rho})\frac{\varepsilon_f B_f - \varepsilon_b B_b}{\varepsilon_f + \varepsilon_b}\cos(\gamma)\Big]\boldsymbol{n}, \end{aligned} \tag{4}$$

$$\boldsymbol{F}_t = PA(1-\tilde{\rho}s)\cos(\gamma)\sin(\gamma)\boldsymbol{t}, \tag{5}$$

where P is the solar radiation pressure, A is the area of the sail, ε_f and ε_b are the front and back emissivities respectively, B_b is the non-Lambertian coefficient of the back surface of the sail respectively, $\tilde{\rho}$ is the reflection coefficient and $\tilde{\sigma}$ is the Stefan-Boltzmann constant.

Thus, equations (4) and (5) can be reduced to

$$\boldsymbol{F}_n = PA\big[a_1\cos^2(\gamma) + a_2\cos(\gamma)\big]\boldsymbol{n}, \tag{6}$$

$$\boldsymbol{F}_t = PAa_3\cos(\gamma)\sin(\gamma)\boldsymbol{t}, \tag{7}$$

where the optical properties of the sail film are given by the coefficients

$$a_1 = 1 + \tilde{\rho}s, \tag{8}$$

$$a_2 = B_f(1-s)\tilde{\rho} + (1-\tilde{\rho})\frac{\varepsilon_f B_f - \varepsilon_b B_b}{\varepsilon_f + \varepsilon_b}, \tag{9}$$

$$a_3 = 1 - \tilde{\rho}s. \tag{10}$$

The total force vector may then be written in terms of normal and transversal components as

$$\begin{aligned} \boldsymbol{F}_{Sail} &= \sqrt{F_n^2 + F_t^2}\boldsymbol{m}, \\ &= PA\sqrt{(a_1\cos(\gamma) + a_2)^2 + a_3^2\sin^2(\gamma)}\cos(\gamma)\boldsymbol{m}, \end{aligned} \tag{11}$$

where $\boldsymbol{m}$ is the unit vector in the direction of the total force, as shown in Figure 1.

For an ideal sail (i.e. a perflect reflector) $\tilde{\rho} = s = 1$, hence $a_1 = 2$, $a_2 = a_3 = 0$, and the total force exerted on the solar sail is given by

$$\boldsymbol{F}_{Sail} = 2PA\cos^2(\gamma)\boldsymbol{n}, \tag{12}$$

with $\boldsymbol{n}$=$\boldsymbol{m}$.

The direction of incidence of photons is defined by a unit vector $\boldsymbol{u}_i$ and the direction of specularly reflected photons by a unit vector $\boldsymbol{u}_r$. The solar sail orientation is defined by a vector $\boldsymbol{n}$ normal to the sail surface with a transverse unit vector $\boldsymbol{t}$ perpendicular to $\boldsymbol{n}$. The angle between $\boldsymbol{m}$ and $\boldsymbol{u}_i$ is defined by the cone angle θ and the angle between $\boldsymbol{m}$ and $\boldsymbol{n}$ is called center-line angle ϕ, and γ is again the pitch angle of the solar sail relative to the Sun-line, as shown in Figure 1.

The center-line angle is given by

$$\begin{aligned} \phi &= \arctan\left(\frac{F_t}{F_n}\right), \\ &= \arctan\left(\frac{a_3\sin(\gamma)}{a_1\cos(\gamma) + a_2}\right), \end{aligned} \tag{13}$$

while the cone angle θ can be calculated using the relation $\gamma = \theta + \phi$, again shown in Figure 1.

The cone angle can then be expressed as

$$\theta = \gamma - \arctan\left(\frac{a_3\sin(\gamma)}{a_1\cos(\gamma) + a_2}\right). \tag{14}$$

EQUATIONS OF MOTION IN PRESENCE OF A SOLAR SAIL

The nondimensional equation of a motion of a solar sail in the rotating frame of reference is described by

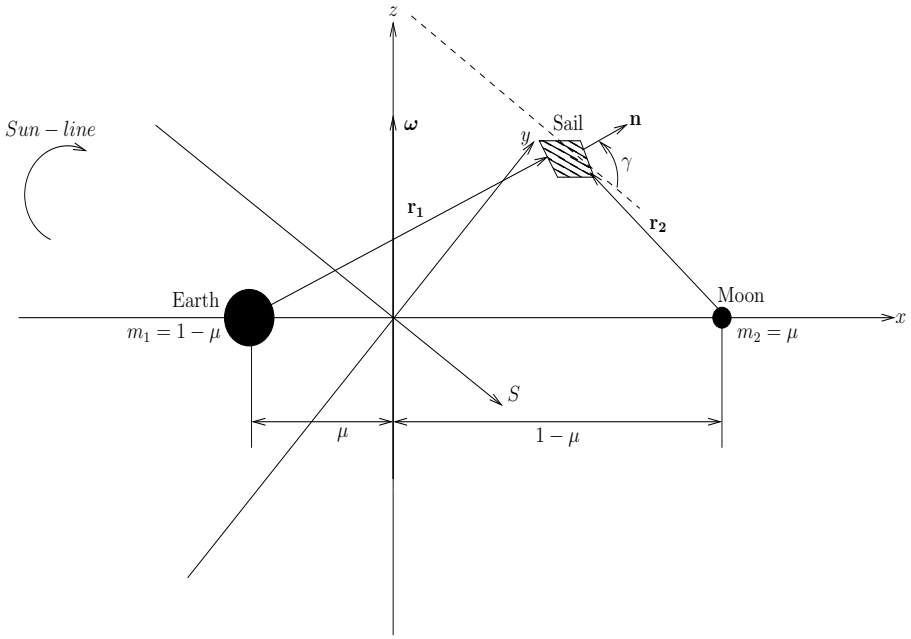

Figure 2. Schematic geometry of the Earth-Moon restricted three-body problem.

$$\frac{d^2\boldsymbol{r}}{dt^2} + 2\boldsymbol{\omega} \times \frac{d\boldsymbol{r}}{dt} + \nabla U(\boldsymbol{r}) = \boldsymbol{a}_S, \tag{15}$$

where $\boldsymbol{\omega} = \omega\hat{\boldsymbol{z}}$ ($\hat{\boldsymbol{z}}$ is a unit vector pointing in the direction $\boldsymbol{z}$) is the angular velocity vector of the rotating frame and $\boldsymbol{r}$ is the position vector of the sail relative to the center of mass of the two primaries. The small annual changes in the inclination of the Sun-line with respect to the plane of the system will not be considered. By introducing the three-body gravitational potential $V(\boldsymbol{r})$ due to the primaries, and the scalar potential $\Phi(\boldsymbol{r})$ to represent the conservative centripetal acceleration, the new modified potential function (pseudo-potential function) is defined by

$$U(\boldsymbol{r}) = V(\boldsymbol{r}) + \Phi(\boldsymbol{r}), \tag{16}$$

where

$$V(\boldsymbol{r}) = -\left[\frac{1-\mu}{r_1} + \frac{\mu}{r_2}\right], \tag{17}$$

$$\Phi(\boldsymbol{r}) = -\frac{1}{2}(x^2 + y^2), \tag{18}$$

with

$$\nabla V(\boldsymbol{r}) = \frac{1-\mu}{r_1^3}\boldsymbol{r}_1 + \frac{\mu}{r_2^3}\boldsymbol{r}_2, \tag{19}$$

$$\nabla \Phi(\boldsymbol{r}) = \boldsymbol{\omega} \times (\boldsymbol{\omega} \times \boldsymbol{r}). \tag{20}$$

The three-body pseudo-potential $U(\boldsymbol{r})$ and the solar radiation pressure acceleration $\boldsymbol{a}_S$ are defined by

$$U(\boldsymbol{r}) = -\left[\frac{1}{2}|\boldsymbol{\omega}\times\boldsymbol{r}|^2 + \frac{1-\mu}{r_1} + \frac{\mu}{r_2}\right], \tag{21}$$

$$\boldsymbol{a}_S = a_0(\boldsymbol{S}\cdot\boldsymbol{n})^2\boldsymbol{n}, \tag{22}$$

where μ is the mass ratio for the Earth-Moon system. The sail position vectors w.r.t. m_1 and m_2 respectively (see Figure 2) are $\boldsymbol{r}_1 = [x+\mu, y, z\,]^T$ and $\boldsymbol{r}_2 = [x-(1-\mu), y, z]^T$, a_0 is the magnitude of the solar radition pressure acceleration exerted on the sail, and the unit vector $\boldsymbol{n}$ denotes the thrust direction. The sail is oriented such that it is always directed along the Sun-line $\boldsymbol{S}$, pitched at an angle γ to provide a constant out-of-plane force. The unit normal to the sail surface $\boldsymbol{n}$ and the Sun-line direction $\boldsymbol{S}$ are given by

$$\boldsymbol{n} = \left[\begin{array}{ccc}\cos(\gamma)\cos(\omega_\star t) & -\cos(\gamma)\sin(\omega_\star t) & \sin(\gamma)\end{array}\right]^T, \tag{23}$$

$$\boldsymbol{S} = \left[\begin{array}{ccc}\cos(\omega_\star t) & -\sin(\omega_\star t) & 0\end{array}\right]^T, \tag{24}$$

where $\omega_\star = 0.923$ is the angular rate of the Sun-line in the corotating frame in a dimensionless synodic coordinate system. The sail normal is chosen to follow the Sun-line and maintain a fixed pitch angle γ, as shown in Figure 2.

LINEARIZED SYSTEM

The dynamics of the sail in the neighborhood of the libration points will now be investigated. The coordinates of the equilibrium point are defined as $\boldsymbol{r}_L = (x_{L_i}, y_{L_i}, z_{L_i})^T$ with $i = 1, \cdots, 5$. Let a small displacement in $\boldsymbol{r}_L$ be $\delta\boldsymbol{r}$ such that $\boldsymbol{r} \to \boldsymbol{r}_L + \delta\boldsymbol{r}$. The equation of motion for the solar sail in the neighborhood of $\boldsymbol{r}_L$ is therefore

$$\frac{d^2\delta\boldsymbol{r}}{dt^2} + 2\boldsymbol{\omega}\times\frac{d\delta\boldsymbol{r}}{dt} + \nabla U(\boldsymbol{r}_L+\delta\boldsymbol{r}) = \boldsymbol{a}_S(\boldsymbol{r}_L+\delta\boldsymbol{r}). \tag{25}$$

Then, retaining only the first-order term in $\delta\boldsymbol{r} = (\xi,\eta,\zeta)^T$ in a Taylor-series expansion, where (ξ,η,ζ) are attached to the Lagrange points, the gradient of the potential and the acceleration can be expressed as

$$\nabla U(\boldsymbol{r}_L+\delta\boldsymbol{r}) = \nabla U(\boldsymbol{r}_L) + \left.\frac{\partial\nabla U(\boldsymbol{r})}{\partial\boldsymbol{r}}\right|_{\boldsymbol{r}=\boldsymbol{r}_L}\delta\boldsymbol{r} + O(\delta\boldsymbol{r}^2), \tag{26}$$

$$\boldsymbol{a}_S(\boldsymbol{r}_L+\delta\boldsymbol{r}) = \boldsymbol{a}_S(\boldsymbol{r}_L) + \left.\frac{\partial\boldsymbol{a}_S(\boldsymbol{r})}{\partial\boldsymbol{r}}\right|_{\boldsymbol{r}=\boldsymbol{r}_L}\delta\boldsymbol{r} + O(\delta\boldsymbol{r}^2). \tag{27}$$

It is assumed that $\nabla U(\boldsymbol{r}_L) = 0$, and the acceleration is constant with respect to the small displacement $\delta\boldsymbol{r}$, so that

$$\left.\frac{\partial\boldsymbol{a}_S(\boldsymbol{r})}{\partial\boldsymbol{r}}\right|_{\boldsymbol{r}=\boldsymbol{r}_L} = 0. \tag{28}$$

The linear variational system associated with the libration points at $\boldsymbol{r}_L$ can be determined by substituting equations (26) and (27) into (25)

$$\frac{d^2\delta\boldsymbol{r}}{dt^2} + 2\boldsymbol{\omega} \times \frac{d\delta\boldsymbol{r}}{dt} + K\delta\boldsymbol{r} = 0, \tag{29}$$

where the matrix K is defined as

$$K = -\left[\frac{\partial \nabla U(\boldsymbol{r})}{\partial \boldsymbol{r}}\bigg|_{\boldsymbol{r}=\boldsymbol{r}_L}\right]. \tag{30}$$

Using matrix notation the linearized equation of motion about the libration point (Equation (29)) can be represented by the inhomogeneous linear system $\dot{\mathbf{X}} = A\mathbf{X} + \boldsymbol{b}(t)$, where the state vector $\mathbf{X} = (\delta\boldsymbol{r}, \delta\dot{\boldsymbol{r}})^T$, and $\boldsymbol{b}(t)$ is a 6×1 vector, which represents the solar sail acceleration.

The Jacobian matrix A has the general form

$$A = \begin{pmatrix} 0_3 & I_3 \\ K & \Omega \end{pmatrix}, \tag{31}$$

where I_3 is a identity matrix, and

$$\Omega = \begin{pmatrix} 0 & 2 & 0 \\ -2 & 0 & 0 \\ 0 & 0 & 0 \end{pmatrix}. \tag{32}$$

For convenience the sail attitude is fixed such that the sail normal vector $\boldsymbol{n}$, points always along the direction of the Sun-line with the following constraint $\boldsymbol{S} \cdot \boldsymbol{n} \geq 0$. Its direction is described by the pitch angle γ relative to the Sun-line, which represents the sail attitude.

EFFECT OF A NON-IDEAL FLAT SAIL MODEL

Considering the non-ideal flat sail model, the total force vector can be written in terms of normal and transversal components as

$$\begin{aligned} \boldsymbol{F}_{Sail} &= \sqrt{F_n^2 + F_t^2}\boldsymbol{m}, \\ &= PA\sqrt{(a_1\cos(\gamma) + a_2)^2 + a_3^2\sin^2(\gamma)}\cos(\gamma)\boldsymbol{m}, \end{aligned} \tag{33}$$

where $\boldsymbol{m}$ is the unit vector in the direction of the total force.

Furthermore, the solar radiation pressure acceleration is given by

$$\begin{aligned} \boldsymbol{a}_{Sail} &= \frac{P}{\sigma}\sqrt{(a_1\cos(\gamma) + a_2)^2 + a_3^2\sin^2(\gamma)}\cos(\gamma)\boldsymbol{m}, \\ &= \frac{a_0}{2}\sqrt{(a_1\cos(\gamma) + a_2)^2 + a_3^2\sin^2(\gamma)}\cos(\gamma)\boldsymbol{m}, \end{aligned} \tag{34}$$

where a_0 is the characteristic acceleration of the non-ideal sail. Thus, the acceleration now acts in direction $\boldsymbol{m}$ rather than normal to the sail surface in direction $\boldsymbol{n}$, as shown for the ideal sail. It is also

Table 1. Optical coefficients for an ideal solar sail and JPL (Jet Propulsion Laboratory) square sail.

	$\tilde{\rho}$	s	ε_f	ε_b	B_f	B_b
$Ideal\ sail$	1	1	0	0	$\frac{2}{3}$	$\frac{2}{3}$
$Square\ sail$	0.88	0.94	0.05	0.55	0.79	0.55

observed that there is a significant deviation in force magnitude between the realistic solar sail and the ideal solar sail model.

The sail optical parameters for a 100×100 m square solar sail will be used to compare the optical solar sail model (realistic solar sail model) to an ideal solar sail, as shown in Figure 3 (a). Then, the force exerted on the realistic solar sail is less than that on the ideal solar sail.

Using the values given in Table 1, the characteristic The characteristic acceleration of the non-ideal sail can be expressed as

$$\begin{aligned} a_0 &= \frac{PA(a_1+a_2)}{m}, \\ &= \frac{P(a_1+a_2)}{\sigma}. \end{aligned} \tag{35}$$

Similarly, the characteristic acceleration for an ideal sail is given by

$$a_0 = \frac{2P}{\sigma}. \tag{36}$$

Recall that the required sail acceleration for a fixed distance ζ_0 is again given by

$$a_0 = \frac{\zeta_0 |U^o_{zz}|}{\cos(\gamma)^2 \sin(\gamma)}. \tag{37}$$

For the realistic solar sail, the out-of-plane distance may then be written approximately as

$$\begin{aligned} \zeta_0^{rss} &= a_0 \cos^2(\gamma)\sin(\gamma)|U^o_{zz}|^{-1}, \\ &= \frac{P(a_1+a_2)}{\sigma}\cos^2(\gamma)\sin(\gamma)|U^o_{zz}|^{-1}. \end{aligned} \tag{38}$$

Similarly, the out-of-plane distance for the ideal solar sail is again given by

$$\zeta_0^{iss} = \frac{2P}{\sigma}\cos^2(\gamma)\sin(\gamma)|U^o_{zz}|^{-1}. \tag{39}$$

Comparing equation (38) and (39), one can see that

$$\begin{aligned} \frac{\zeta_0^{rss}}{\zeta_0^{iss}} &= \frac{a_1+a_2}{2}, \\ &\approx 0.9081. \end{aligned} \tag{40}$$

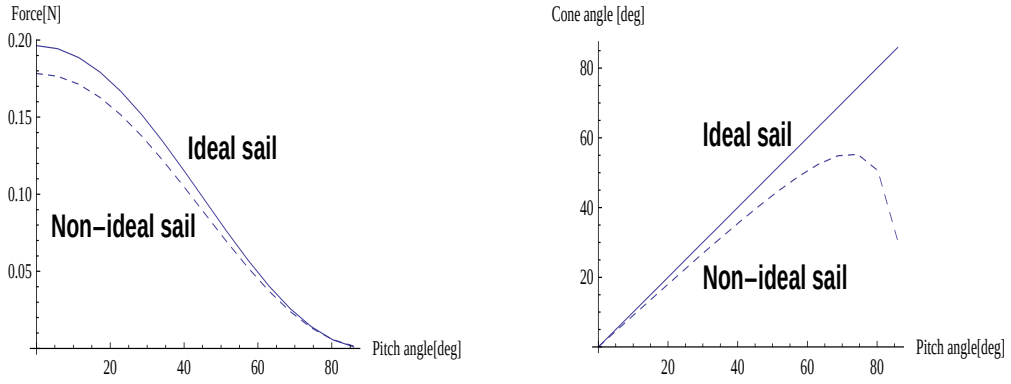

(a) (b)

Figure 3. (a) Force exerted on a 100×100 m ideal square solar sail and non-ideal square solar sail at 1 AU; (b) Cone angle for an ideal solar sail and non-ideal solar sail model.

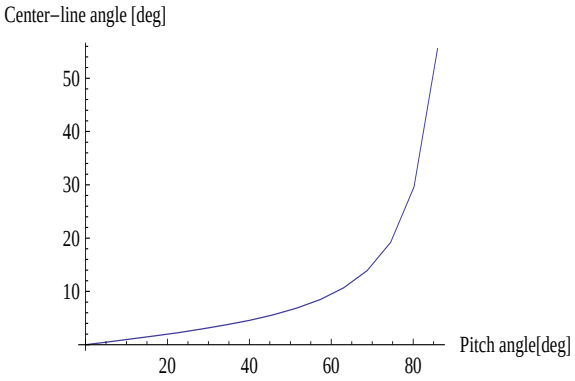

Figure 4. Center-line angle for a non-ideal solar sail model.

Therefore, the out-of-plane distance due to the realistic solar sail is less by a factor of order 0.0919 than that on the ideal solar sail. The main effect of the non-perfect sail is to reduce the out-of-plane displacement distance which may be achieved for a given characteristic acceleration.

Again, the realistic solar sail model can be compared with an ideal solar sail using the cone angle, as shown in Figure 3 (b). Most importantly, the realistic square solar sail model can only direct its force vector to a maximum cone angle of $55.5°$ (corresponding to a sail pitch angle of $72.6°$) due to the center-line effect. It should be noted that the center-line angle for a perfectly reflecting solar sail vanishes since the force vector is always directed normal to the sail surface, while the non-perfect solar sail has a center-line angle due to the optical absorption. Then, Figure 4 shows the variation of the centerline angle as a function of the pitch angle.

Equation (38) is approximate since the angle γ is the pitch angle, while for a realistic sail, one should use the cone angle, but the difference will be small.

ONE-MONTH ORBITS

This section is now concerned with the numerical computation of displaced periodic orbits around the Lagrange points in the Earth-Moon system. For example, the numerical nonlinear results for the Lagrange points L_4 (Figure 5 (a)), and L_5 (Figure 7 (b)) demonstrate, that displaced periodic orbits appear in their vicinity with a period of 28 days (synodic lunar month).

Furthermore, the numerically integrated nonlinear (solid line) equations match the linear analytic solutions (dashed line) for a small displaced orbit (Figure 6, 8 (a) for L_4 and Figure 6, 8 (b) for L_5). Good agreement was obtained between the linear analytic solutions (dashed line) and the numerical nonlinear solutions (solid line) over the entire period.

It was found that for a given displacement distance above/below the Earth-Moon plane it is easier by a factor of order 3.19 to do so at L_4/L_5 compared to L_1/L_2 - ie. for a fixed sail acceleration the displacement distance at L_4/L_5 is greater than that at L_1/L_2. In addition, displaced L_4/L_5 orbits are passively stable, making them more forgiving to sail pointing errors than highly unstable orbits at L_1/L_2.

The drawback of the new family of orbits at L_4 and L_5 is the increased telecommunications path-length, particularly the Moon-L_4 distance compared to the Moon-L_2 distance.

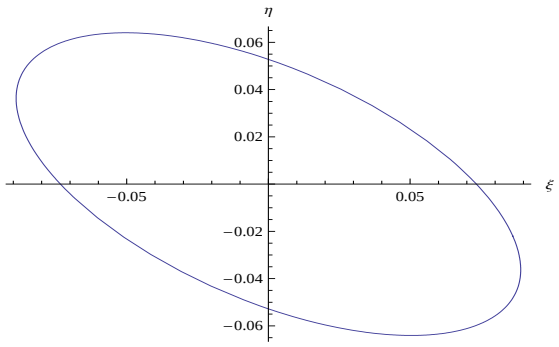

(a)

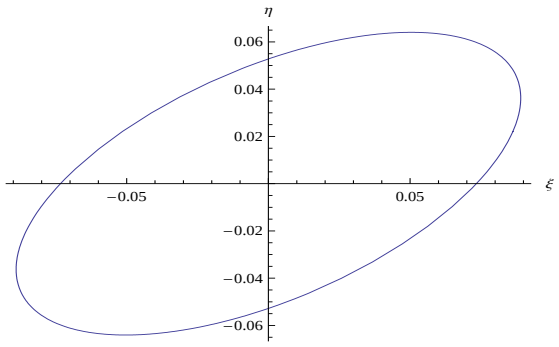

(b)

Figure 5. (a) **Periodic orbits at linear order around** L_4**;** (b) **Periodic orbits at linear order around** L_5 **(**$\zeta = 200\ km$**).**

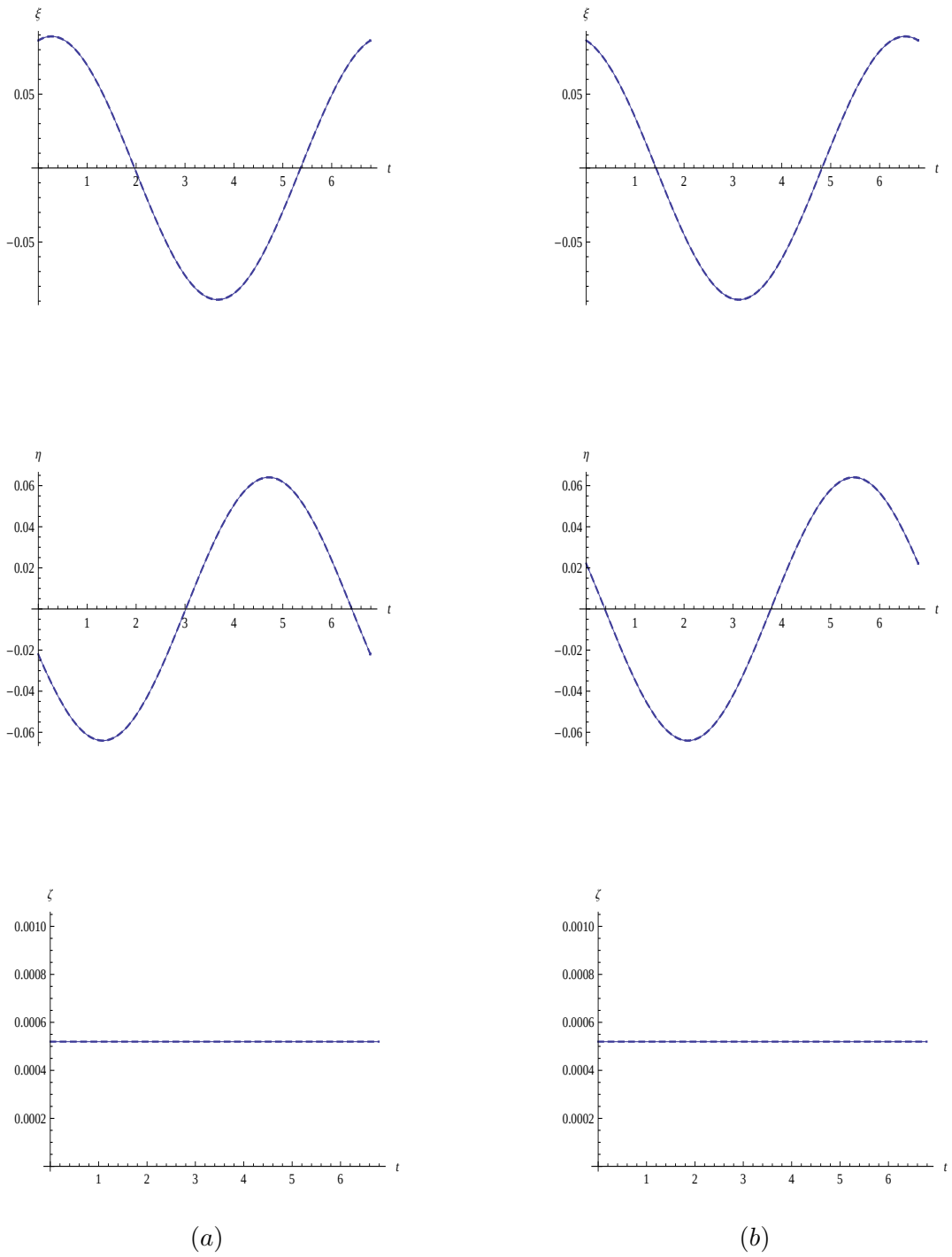

(a) (b)

Figure 6. (a) **Comparison between the analytical (dashed line) and nonlinear (solid line) results (L_4) for a constant displacement distance of $\zeta = 200\ km$; (b) Comparison between the analytical (dashed line) and nonlinear (solid line) results (L_5 for a constant displacement distance of $\zeta = 200\ km$).**

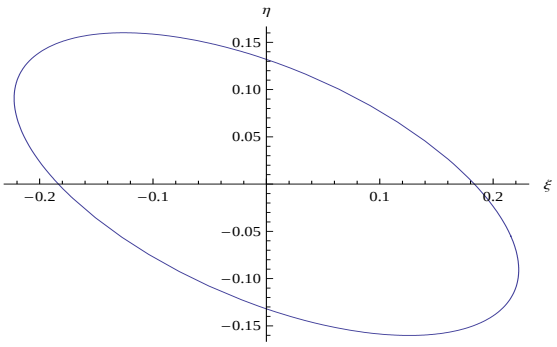

(a)

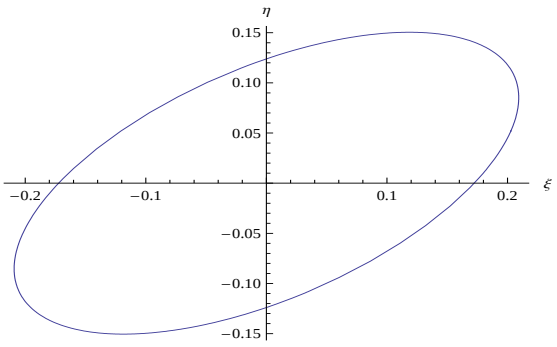

(b)

Figure 7. (a) **Periodic orbits at linear order around** L_4**;** (b) **Periodic orbits at linear order around** L_5 **(**$\zeta = 500\ km$**).**

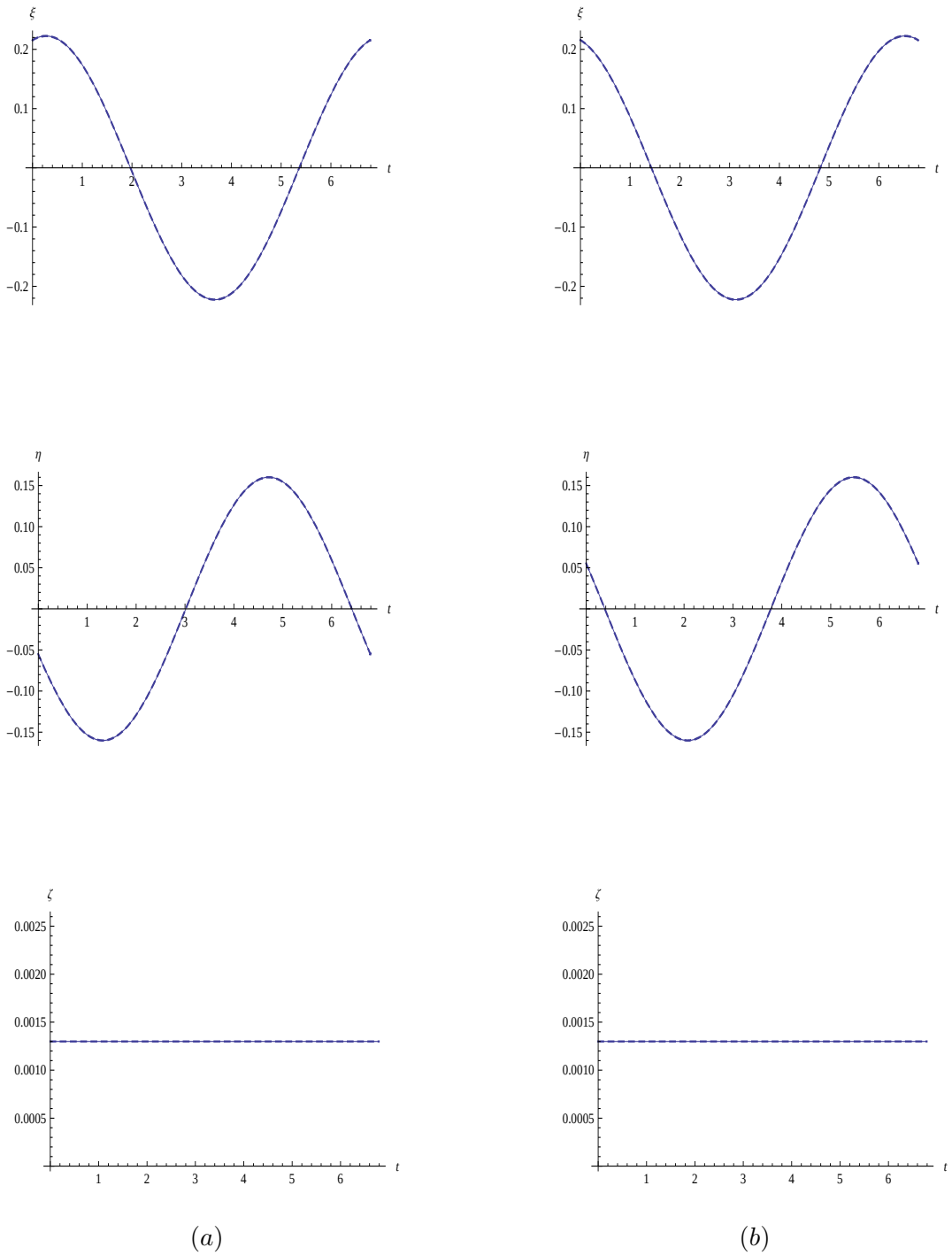

(a) (b)

Figure 8. (a) **Comparison between the analytical (dashed line) and nonlinear (solid line) results (L_4) for a constant displacement distance of $\zeta = 500\ km$; (b) Comparison between the analytical (dashed line) and nonlinear (solid line) results (L_5) for a constant displacement distance of $\zeta = 500\ km$.**

CONCLUSIONS

In this paper a novel family of displaced periodic orbits at linear order using solar sail propulsion have been presented from the non-autonomous Earth-Moon system. Using the linearized equations of motion around the Lagrange points, periodic orbits that are displaced can be derived, which will be interesting for future mission design for lunar communication applications. Thereafter, the resulting effects of the non-ideal flat sail model have been computed and compared with an ideal solar sail. It is observed that there is a significant deviation in force magnitude between the realistic solar sail and the ideal solar sail model. Then, the force exerted on the realistic solar sail is less than that on the ideal solar sail. Therefore, the out-of-plane distance due to the realistic solar sail is less by a factor of order 0.0919 than that on the ideal solar sail. Again, the main effect of the non-perfect sail is to reduce the out-of-plane displacement distance which may be achieved for a given characteristic acceleration.

REFERENCES

[1] J. Simo and C. R. McInnes, "Solar sail trajectories at the Earth-Moon Lagrange points," *In* 59^{th} *International Astronautical Congress*, Glasgow, Scotland, 29 Sep - 03 Oct 2008. Paper IAC-08.C1.3.13.

[2] J. Simo and C. R. McInnes, "Solar Sail Orbits at the Earth-Moon Libration points," *Communications in Nonlinear Science and Numerical Simulation*, Vol. 14, No. 12, December 2009, pp. 4191–4196.

[3] J. Simo and C. R. McInnes, "Designing Displaced Lunar Orbits Using Low-Thrust Propulsion," *Journal of Guidance, Control and Dynamics*, Vol. 33, No. 1, January-February 2010.

[4] J. Simo and C. R. McInnes, "Displaced solar sail orbits: Dynamics and applications," *In* 20^{th} *AAS/AIAA Space Flight Mechanics Meeting*, San Diego, California, February 14-17, 2010. AAS 10-222.

[5] J. Simo and C. R. McInnes, "Tracking Unstable Periodic Orbits in the Circular Restricted Three-Body Problem," *Workshop on Applications on Control theory to Astrodynamics problems, Surrey, England, April 26-27, 2010*.

[6] J. Simo and C. R. McInnes, "Feedback Stabilization of Displaced Periodic Orbits: Application to Binary Asteroids," *Acta Astronautica*, Vol. 96, March-April 2014, pp. 106–115.

[7] C. R. McInnes, *Solar sailing: technology, dynamics and mission applications*. London: Springer Praxis, 1999.

[8] M. Leipold and M. Götz, "Hybrid Photonic/Electric Propulsion," *Kayser-Threde, TR SOL4- TR-KTH-0001*, Munich, Jan. 2002, ESA Contract No. 15334/01/NL/PA.

[9] G. Mengali and A. A. Quarta, "Trajectory Design with Hybrid Low-Thrust Propulsion system," *Journal of Guidance, Control, and Dynamics*, Vol. 30, No. 2, March-April 2007, pp. 419–426.

[10] B. Wie, "Thrust Vector Control Analysis and Design for Solar-Sail Spacecraft," *Journal of Spacecraft and Rockets*, Vol. 44, No. 3, May-June 2007, pp. 545–557.

[11] V. L. Coverstone and J. E. Prussing, "Technique for Escape from Geosynchronous Transfer Orbit Using a Solar Sail," *Journal of Guidance, Control and Dynamics*, Vol. 26, No. 4, July-August 2003, pp. 628–634.

[12] T. Cichan and R. G. Melton, "Optimal Trajectories for Non-Ideal Solar Sails," *Advances in the Astronautical Sciences*, Vol. 109, No. 3, 2001, pp. 2381–2391.

[13] B. Dachwald, W. Seboldt, and B. Häusler, "Performance Requirements for Near-Term Interplanetary Solar Sailcraft Missions," 6^{th} *International Symposium on Propulsion for Space Transportation of the XXIst Century*, Versailles, France, May 2002.

[14] H. Baoyin and C. McInnes, "Solar sail halo orbits at the Sun-Earth artificial L_1 point," *Celestial Mechanics and Dynamical Astronomy*, Vol. 94, No. 2, 2006, pp. 155–171.

[15] J. Simo and C. R. McInnes, "Stabilization of Displaced Periodic Orbits in the Solar Sail Restricted Three-Body Problem," *presented at the SIAM Conference on Applications of Dynamical Systems (DS09)*, Snowbird, Utah, May 17 - 21, 2009.

[16] J. Simo and C. R. McInnes, "Asymptotic Analysis of Displaced Lunar Orbits," *Journal of Guidance, Control and Dynamics*, Vol. 32, No. 5, September-October 2009, pp. 1666–1671.

[17] J. Simo and C. R. McInnes, "Analysis and Control of Displaced Periodic Orbits in the Earth-Moon System," *In* 60^{th} *International Astronautical Congress*, Daejeon, Republic of Korea, 12 - 16 October 2009. IAC-09.C1.2.4.

[18] J. Simo and C. R. McInnes, "Displaced Periodic Orbits with Low-Thrust Propulsion in the Earth-Moon System," *In* 19^{th} *AAS/AIAA Space Flight Mechanics Meeting*, Savannah, Georgia, February 8 - 12, 2009. AAS 09-153.

[19] M. Ozimek, D. Grebow, and K. Howell, "Solar Sails and Lunar South Pole Coverage," *In AIAA/AAS Astrodynamics Specialist Conference and Exhibit*, Honolulu, Hawaii,August 2008. Paper AIAA-2008-7080.

[20] G. G. Wawrzyniak and K. Howell, "Numerical Techniques for Generating and Refining Solar Sail Trajectories," *Advances in Space Research*, Vol. 48, 2011.

[21] G. Gómez, A. Jorba., J.Masdemont, and C. Simó, *Dynamics and Mission Design Near Libration Points*, Vol. III, IV. Singapore.New Jersey.London.Hong Kong: World Scientific Publishing Co.Pte.Ltd, 2001.

[22] R. Farquhar and A. Kamel, "Quasi-periodic orbits about the translunar libration point," *Celestial Mechanics*, Vol. 7, 1973, pp. 458–473.

[23] J. Breakwell and J. Brown, "The 'halo' family of 3-dimensional periodic orbits in the Earth-Moon restricted 3-body problem," *Celestial Mechanics*, Vol. 20, 1979, pp. 389–404.

[24] F. Vonbun, ""A Humminbird for the L_2 Lunar Libration Point"," *Nasa TN-D-4468*, April 1968.